

# Graphene oxide nanosheets reshape synaptic function in cultured brain networks

Rossana Rauti<sup>†</sup>, Neus Lozano<sup>§</sup>, Veronica León<sup>‡</sup>, Denis Scaini<sup>#</sup>, Mattia Musto<sup>°</sup>, Ilaria Rago<sup>#</sup>, Francesco P. Ulloa Severino<sup>°</sup>, Alessandra Fabbro<sup>||</sup>, Loredana Casalis<sup>#</sup>, Ester Vázquez<sup>‡</sup>, Kostas Kostarelos<sup>§</sup>, Maurizio Prato<sup>||&†</sup> and Laura Ballerini<sup>°\*</sup>

<sup>†</sup>Life Science Department, University of Trieste, 34127 Trieste, Italy

<sup>§</sup>Nanomedicine Lab, School of Medicine and National Graphene Institute, Faculty of Medical & Human Sciences, University of Manchester, M13 9PL Manchester, United Kingdom

<sup>‡</sup>Departamento de Química Orgánica, Facultad de Ciencias y Tecnologías Químicas-IRICA Universidad de Castilla La-Mancha, 13071 Ciudad Real, Spain

<sup>#</sup>ELETTRA Synchrotron Light Source, 34149 Trieste, Italy

<sup>°</sup>International School for Advanced Studies (SISSA), 34136 Trieste, Italy

<sup>||</sup>Department of Chemical and Pharmaceutical Sciences, University of Trieste, 34127 Trieste, Italy

<sup>&</sup>CIC BiomaGUNE, Parque Tecnológico de San Sebastián, Paseo Miramón, 182, 20009 San Sebastián (Guipúzcoa), Spain

<sup>†</sup>Basque Foundation for Science, Ikerbasque, Bilbao 48013, Spain

\* Corresponding authors: Laura Ballerini International School for Advanced Studies (SISSA) via Bonomea 265 I-34136 Trieste [laura.ballerini@sissa.it](mailto:laura.ballerini@sissa.it) ; [prato@units.it](mailto:prato@units.it)

## 1 **Abstract**

2 Graphene offers promising advantages for biomedical applications. However, adoption of  
3 graphene technology in biomedicine also poses important challenges in terms of understanding  
4 cell responses, cellular uptake or the intracellular fate of soluble graphene derivatives. In the  
5 biological microenvironment graphene nanosheets might interact with exposed cellular and  
6 subcellular structures resulting in unexpected regulation of sophisticated biological signaling.  
7 More broadly, biomedical devices based on the design of these 2D planar nanostructures for  
8 interventions in the central nervous system (CNS) requires an accurate understanding of their  
9 interactions with the neuronal milieu. Here, we describe the previously unreported ability of  
10 graphene oxide nanosheets to down-regulate neuronal signaling without affecting cell viability.

## 11 **Keywords**

12 Nanotechnology; graphene; patch-clamp; synaptic terminals; exocytosis; FMI-43;  
13 microvesicles.  
14

## 15 **Text**

16 Graphene is a 2D plate-like material consisting of sp<sup>2</sup>-hybridized carbon atoms organized  
17 in a hexagonal lattice and characterized by, among other properties, high electrical conductivity  
18 and mechanical flexibility<sup>1,3</sup>. In addition to the successful exploitation of graphene and  
19 graphene-based materials in an increasing number of industrial products, current applications of  
20 graphene hold the potential to revolutionize specific areas of medicine<sup>2,6</sup>. Biomedical  
21 developments in general, and in neurology in particular, are focusing on few-layer graphene  
22 sheets to manufacture novel bio-devices, including biosensors, interfaces, tissue scaffolds, drug  
23 delivery and gene therapy vector systems<sup>4</sup>. Successful design of multifunctional neuro-devices  
24 based on graphene will expose brain cells and neuronal circuits directly to this material by  
25 injection or implantation<sup>4,7</sup>. In this context, the exploration of the interactions between graphene  
26 nano- and micro-sheets with the sophisticated signaling machinery of nerve cells, with a  
27 particular focus on potential graphene flake interactions with the hydrophobic membrane  
28 domains, is of great importance<sup>1,8,9</sup>. Such interactions may favor graphene translocation, or  
29 adhesion to cell membranes<sup>8,10</sup>, potentially interfering with exquisite membrane activities, such  
30 as the exocytic and endocytic trafficking systems, crucial to physiological synaptic  
31 transmission<sup>8,11</sup>.

32 Here we explore for the first time by patch clamp and fluorescence imaging the ability of  
33 graphene (GR) and graphene oxide (GO) nanosheets to interfere with synaptic signaling once  
34 hippocampal cultured neurons are exposed for one week to a growth medium containing thin  
35 sheets of such materials at 1 or 10  $\mu\text{g}/\text{mL}$  (concentrations reported not to induce cell death<sup>12-14</sup>).  
36

1 We further investigated whether, in the absence of explicit cell toxicity, such materials affected  
2 the ability of astrocytes to release synaptic-like microvesicles<sup>15</sup> (MV) in pure glial cultures. Our  
3 results describe the potential of GO nanosheets to alter different modes of inter-neuronal  
4 communication systems in the CNS hinting at opportunities for novel neuromodulatory  
5 applications or highlighting subtle, but potentially unwanted, subcellular interactions.  
6

## 7 **Results and Discussion**

8 To address the issue of prolonged exposure of a functional brain network to graphene  
9 sheets we used different materials. Graphene oxide sheets of large and small lateral dimensions  
10 (l-GO and s-GO, respectively) were synthesized using a modified-Hummers method (see  
11 Supporting Information). Following the reaction, the GO-gel like upper layer was extracted  
12 carefully by using warm water, resulting in the large GO (l-GO). Final concentrations ranged  
13 between 1 and 2mg/mL were obtained with a yield of ca. 10%. l-GO was freeze-dried,  
14 reconstituted in water for injection, sonicated for 5 mins and centrifuged at room temperature to  
15 generate the small GO (s-GO). The lateral dimension of GO sheets was controlled by drying and  
16 sonicating the l-GO to obtain the s-GO sheets, that were always at least one order of magnitude  
17 smaller, without introducing any significant changes among their surface properties (see Table  
18 S1).

19 The GO dispersions in aqueous media were homogenous, of brownish color and stable at  
20 room temperature for more than 6 months. The physicochemical characterization of the l-GO and  
21 s-GO dispersions is shown in Figure 1 (a-f), and in the Supporting Information Figure S1 and S2.  
22 Their structural properties (lateral dimension and thickness) were studied by optical microscopy,  
23 transmission electron microscopy (TEM) and atomic force microscopy (AFM). Optical  
24 properties were studied by UV-Vis and fluorescence spectroscopy. Raman spectroscopy and  
25 laser Doppler electrophoresis (measuring  $\zeta$ -potential) were used to assess the surface properties  
26 of the GO materials. Their Raman spectrum showed D and G bands at 1319  $\text{cm}^{-1}$  and 1596  $\text{cm}^{-1}$ ,  
27 respectively, characteristic of most poly-aromatic hydrocarbons. The D to G band intensity ratio  
28 (ID/IG) was calculated at 1.3, corresponding to the metric of disorder in the graphitic structure.  
29 The surface charge measured with a Zetasizer instrument showed an average  $\zeta$ -potential of -50  
30 mV, indicating flakes of high negative surface charge. To elucidate the degree of surface  
31 functionalization, thermo-gravimetric analysis (TGA) and X-ray photoelectron spectroscopy  
32 (XPS) survey spectra were performed to quantify the purity of the GO (> 99%) and the C:O ratio  
33 XPS high resolution C1s spectra were recorded to elucidate the contribution of individual  
34 functional groups such as carboxylic, carbonyl, epoxide and hydroxyl (Table S2b). All fittings  
35 shown were performed using the CasaXPS software and the different regions were assigned  
36 according to Nist XPs and lasurface databases. Deconvolution XPS spectra and assignment of

1 the functional groups indicated that hydroxyls were the least abundant species in the GO material  
2 produced (see also Supporting Information, Table S2a).

3 Aqueous dispersions of graphene (GR) flakes were prepared using ball-milling for the  
4 exfoliation of graphite through interaction with melamine, as previously described<sup>16,17</sup> (see  
5 Supporting Information). Due to the GR preparation process, graphene dispersions can contain  
6 traces of melamine. In order to determine the exact amount of these traces, final graphene  
7 dispersions (0.09 mg/mL) were evaluated by elemental analysis indicating 0.9 ppm of melamine.  
8 Experiments that involved incubation in neurons also included controls exposed to equal  
9 amounts of melamine alone (see Supporting Information). The physicochemical characterization  
10 of GR dispersions is shown in Figure S3. The lateral size, studied by TEM, was found to range  
11 between 500nm-3 $\mu$ m (Figure S3a-b). Optical properties were studied by UV-Vis absorption  
12 spectroscopy. Dispersions were diluted and their UV-Vis absorption spectra were recorded  
13 (Figure S3). The spectra are featureless in the Vis-NIR region, as expected. The absorbance at  
14 660 nm, divided by cell length, is plotted against the concentration exhibiting Lambert-Beer  
15 behavior (Figure S3d). Raman spectroscopy revealed differences between the GO and GR.  
16 Graphene exhibits G and 2D modes around 1573 and 2700 cm<sup>-1</sup>, that satisfy Raman selection  
17 rules, while the D peak, around 1345 cm<sup>-1</sup> requires a defect for its activation (Figure S3e). The  
18 D to G band intensity ratio was calculated at different locations, giving a significant low value  
19 (0.22) in comparison with GO. TGA was also used to quantify the functionalization degree of  
20 GR. The low weight loss observed in GR (7%) corroborated the low quantity of oxygen groups  
21 generated by the exfoliation process (Figure S3f).

22 We used hippocampal neurons isolated and cultured for 8-10 days *in vitro* (DIV).  
23 Primary neuronal cultures were incubated at 2 DIV in the presence of GR or s-GO (at 1  $\mu$ g/mL  
24 and 10  $\mu$ g/mL; see Supporting Information) maintained for 6 to 8 days and afterwards visually  
25 identified neurons were patch clamped under voltage clamp. Hippocampal neuron maturation  
26 and viability were assessed using single-cell recordings (see Supporting Information) to measure  
27 the cell passive membrane properties that are accepted indicators of neuronal health<sup>18-20</sup> that  
28 allowed comparison among the recorded cells. These parameters (membrane capacitance and  
29 input resistance) displayed similar values in all treatment conditions (summarized in Table 1).

30  
31 **Table 1.** Neuronal passive membrane properties upon GR and s-GO exposure (1  $\mu$ g/mL and 10  $\mu$ g/mL  
32 respectively).  
33

	Capacitance (pF)	Input Resistance (M $\Omega$ )
Control, <sub>n=24</sub>	59 $\pm$ 4	976 $\pm$ 138

Melamine <sub>10</sub> n=28	46 ± 5	1036 ± 132
s-GO <sub>1</sub> n=27	62 ± 8	876 ± 145
GR <sub>1</sub> n=30	50 ± 5	1029 ± 161
Control <sub>10</sub> n=20	57 ± 7	744 ± 82
Melamine <sub>10</sub> n=25	72 ± 16	717 ± 106
s-GO <sub>10</sub> n=18	67 ± 6	997 ± 156
GR <sub>10</sub> n=25	59 ± 18	1223 ± 501

1

2

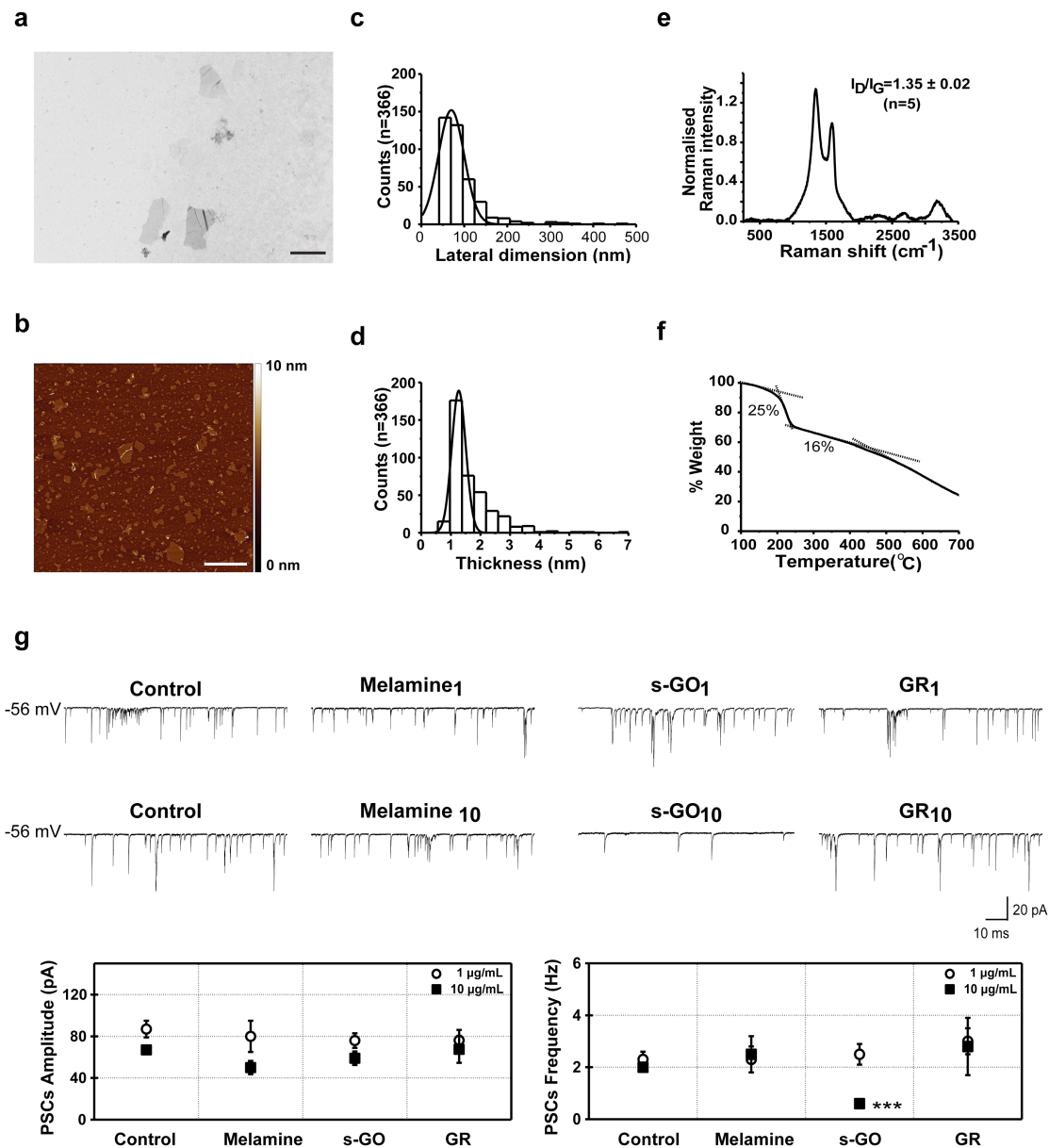
3

4

5

To investigate synapse formation and activity after *in vitro* growth of neurons, we monitored the occurrence of spontaneous postsynaptic currents (PSCs). The appearance of PSCs provided clear evidence of functional synapse formation and it is a widely accepted index of network efficacy<sup>21,22</sup>.

1 **Figure 1**



2  
 3 **Figure 1.** *Characterization of small graphene oxide (s-GO) of biological-grade; graphene oxide exposure at high*  
 4 *concentration influences synaptic function.* In (a-f) physicochemical characterization of s-GO: (a) TEM micrograph  
 5 (scale bar 1  $\mu\text{m}$ ). (b) AFM height image (scale bar 1  $\mu\text{m}$ ), (c) lateral dimension distribution and (d) thickness  
 6 distribution analysis. (e) Normalized Raman spectrum. (f) TGA analysis. In (g) graphene oxide exposure at high  
 7 concentration influences synaptic function. Spontaneous synaptic activity recorded from hippocampal cultures in  
 8 control, melamine, s-GO and GR-treated cultures at 1  $\mu\text{g/mL}$  (top traces) and 10  $\mu\text{g/mL}$  (bottom traces) grown for 8  
 9 to 10 DIV. PSCs were detected at -56 mV holding potential. Bottom plots represent pooled data and summarize  
 10 average PSCs amplitude and frequency: note the reduction in s-GO-treated (10  $\mu\text{g/mL}$ , final concentration) of  
 11 PSCs frequency (\*\*\*) =  $P < 0.001$  Student's test, data are mean  $\pm$  SEM).  
 12

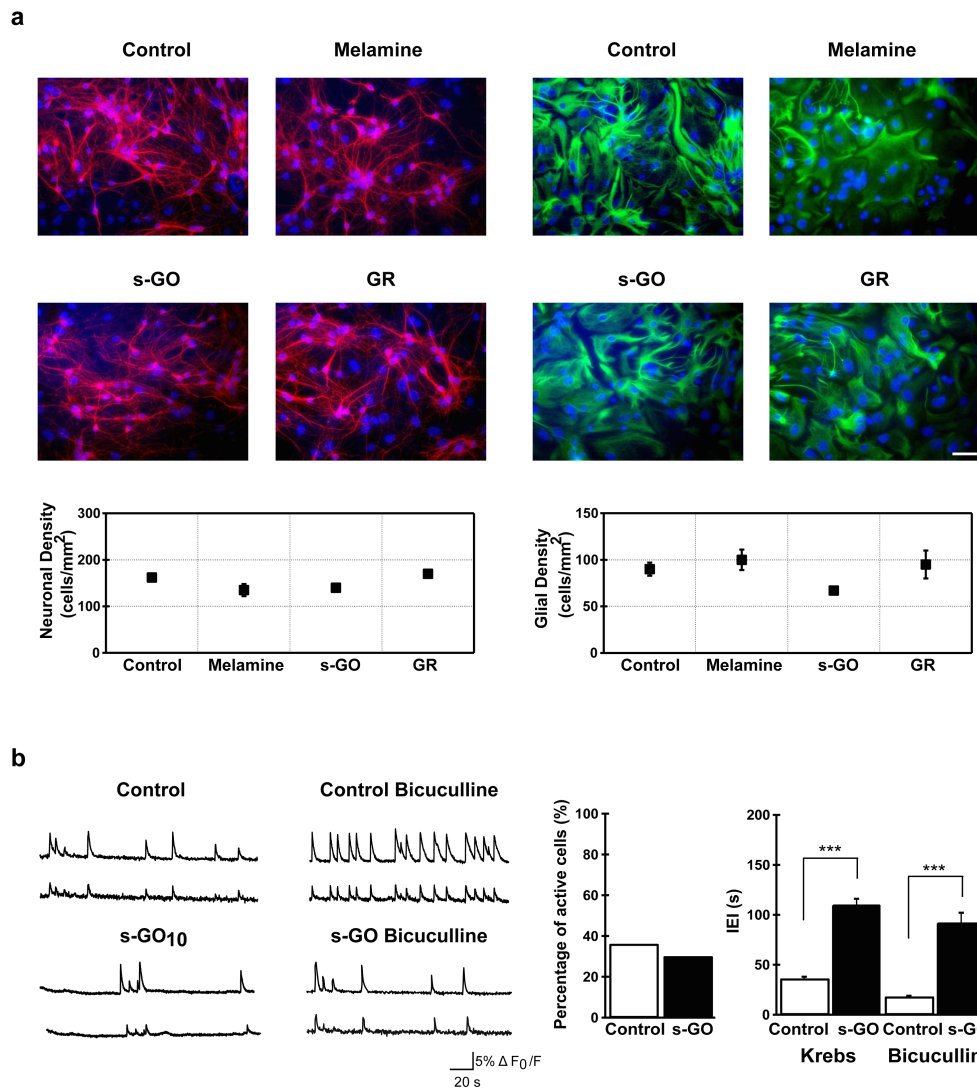
13 Figure 1g, shows representative current tracings of the recorded electrical activity. In  
 14 neurons exposed to low (1  $\mu\text{g/mL}$ ) s-GO and GR, spontaneous synaptic activity was not

1 affected. In fact, measured PSC amplitude and frequency in s-GO and GR ( $79 \pm 7$  pA and  $2.5 \pm$   
2  $0.4$  Hz  $n=27$  and  $77 \pm 8$  pA and  $3 \pm 0.5$  Hz,  $n= 30$ , respectively) were comparable to the  
3 corresponding control and control-melamine values ( $87 \pm 8$  pA and  $2.3 \pm 0.3$  Hz, control,  $n=24$ ;  
4  $80 \pm 15$  pA and  $2.3 \pm 0.5$  Hz melamine  $n= 28$ ; plots in Figure 1 (g)). In all tests, cell parameters  
5 measured in melamine were comparable to those expressed by control neurons (Figure 1 (g)  
6 bottom plots), thus the impact on cells of such a contaminant at the estimated concentration is  
7 negligible.

8         When investigating the impact of higher graphene doses ( $10 \mu\text{g/mL}$ ) we detected a  
9 significant difference ( $P < 0.001$ ; Student's t-test) in PSC frequency when comparing control  
10 neurons ( $2.0 \pm 0.1$  Hz control,  $n= 20$ ) with s-GO treated ones ( $0.6 \pm 0.1$  Hz,  $n= 18$ ), while in  
11 melamine and GR, PSC frequency values remained unchanged ( $2.5 \pm 0.7$  Hz melamine,  $n= 25$   
12 and  $2.8 \pm 1.1$  Hz GR;  $n= 25$ ). In all treatments studied, the amplitude values of the PSCs were  
13 never affected (data are summarized in Figure 1 (g) plots). We further tested synaptic responses  
14 when neurons were treated ( $1$  and  $10\mu\text{g/mL}$ ) with a commercially available GO provided by an  
15 industrial partner (A-GO; Supporting Information and Figures S4). Similar reduction in PSC  
16 frequency (Figure S5) was detected that validated the observation that GO nanosheets,  
17 differently to GR flakes, specifically interfered with synapses in cultured neurons, regardless of  
18 the starting material.

19

1 **Figure 2**



2  
3 **Figure 2.** *s-GO* exposure at high concentration impaired network activity without changing network size. In (a)  
4 immunofluorescence images are shown to visualize neurons and glial cells in the 4 different conditions (anti  $\beta$ -  
5 tubulin III, in red, left panels; anti-GFAP, in green, right panels, in all nuclei are visualized by DAPI in blue)  
6 (samples are for the 10  $\mu\text{g}/\text{mL}$  protocol; scale bar 50  $\mu\text{m}$ ). The plots summarize neuronal (left) and glial (right)  
7 densities in all conditions. In (b) repetitive  $\text{Ca}^{2+}$ -oscillations spontaneously (left panel) or bicuculline-induced (right  
8 panel) recorded in hippocampal cultures at 8 to 10 DIV (from each field sample recordings of 2 cells were selected).  
9 Histograms summarize the percentage of spontaneous active cells (middle) and the average values of the inter-event-  
10 interval (IEI; right) in standard saline (Krebs) and in the presence of bicuculline (\*\*\*) =  $P < 0.001$  Student's *t*-test,  
11 data are mean  $\pm$  SEM).

12  
13 The impact of 10  $\mu\text{g}/\text{mL}$  *s-GO* on synaptic activity was not related to a decreased  
14 number of surviving neurons in the presence of *s-GO*. In fact, we determined the cellular  
15 composition of control and *s-GO* treated hippocampal cultures using immunofluorescence  
16 markers<sup>23</sup> for astrocytes (GFAP) and neurons ( $\beta$ -tubulin III). We observed both  $\beta$ -tubulin III and  
17 GFAP immunoreactive cells in all growing conditions (Figure 2 (a)) and both cell groups were  
18 represented in a comparable proportion in all treatment groups (quantified by measuring the cell



1 density in Figure 2 (a), (n=13 visual field per condition, 3 different culture series). Thus s-GO at  
2 higher concentrations specifically altered synapse formation and/or function without affecting  
3 cell survival or the global network size.

4 To gain more insight into such processes we further investigated s-GO-treated (10  
5  $\mu\text{g}/\text{mL}$ ) cultures. We specifically addressed the distribution of neuronal excitation by measuring  
6 the activity of small clusters of neurons with fluorescence calcium imaging<sup>23,25</sup>. On average  $7 \pm 2$   
7 fluorescent neurons (n=26 fields), stained with the membrane permeable  $\text{Ca}^{2+}$  dye Fura-2-AM  
8 (see Supporting Information), were simultaneously visualized in the recorded field ( $120 \times 160$   
9  $\mu\text{m}^2$ ). We compared and characterized the cell ability to generate repetitive  $\text{Ca}^{2+}$  oscillations<sup>23,25</sup>. In  
10 control conditions all recorded fields (n=8) displayed active cells, while in s-GO treated cells  
11 56% (n=10 out of 18) of the recorded fields did not display detectable cell activity. However, in  
12 the remaining s-GO fields (n=8), we found an amount of neurons that were spontaneously  
13 generating repetitive  $\text{Ca}^{2+}$  oscillations comparable to that measured in controls (Figure 2 (b), 36%  
14 in control, 20 out of 56 neurons, n=8 active fields and 30% in s-GO-treated, 18 out of 60  
15 neurons, n=8 active fields).

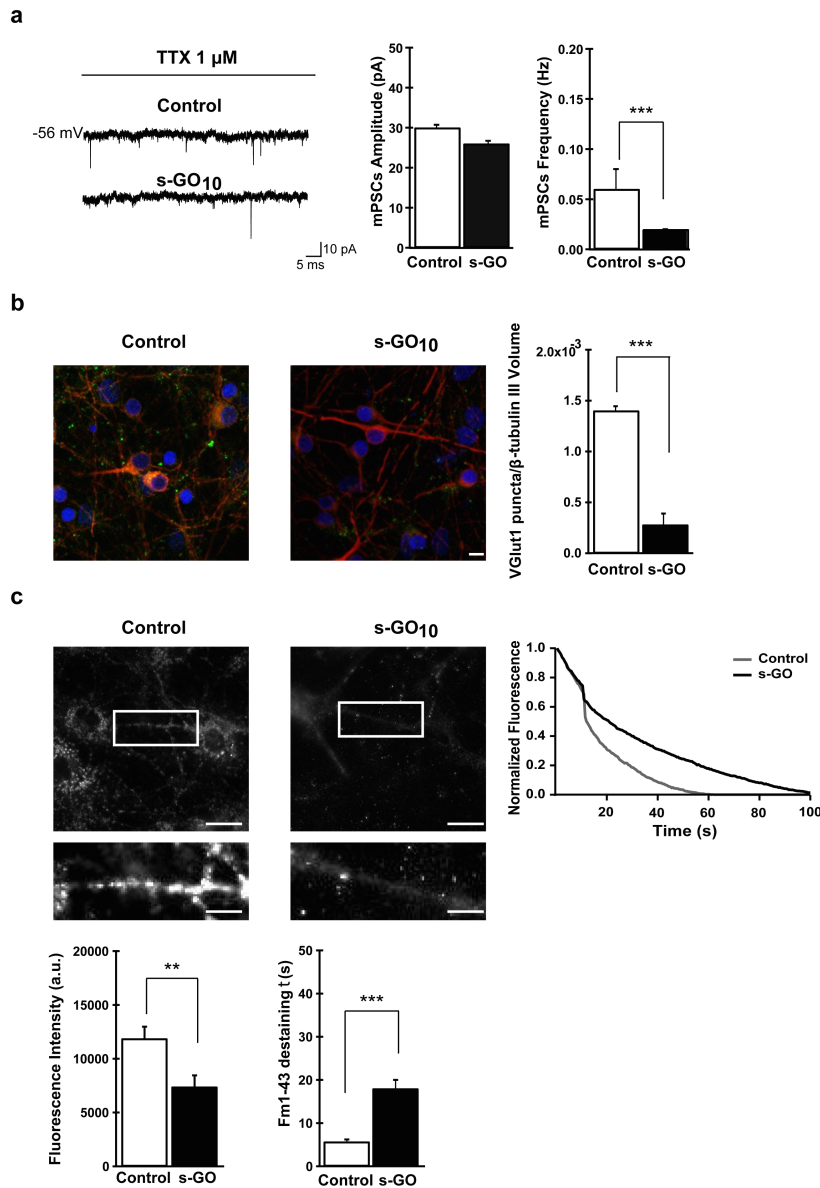
16 Figure 2 (b) traces represent fluorescence recordings from active fields in control and s-  
17 GO-treated cultures (2 sampled cells in each field). Episodes usually comprised spontaneous  
18 bursts of activity, fully blocked by tetrodotoxin (TTX, a blocker of voltage-gated, fast  $\text{Na}^+$   
19 channels) applications ( $1 \mu\text{M}$ ; n= 8 fields, control and s-GO-treated; not shown). Control  $\text{Ca}^{2+}$   
20 oscillations displayed an inter-event interval (IEI) of  $36 \pm 2 \text{ s}$  (n=20 cells) that was significantly  
21 lower ( $P < 0.001$ ; Student's t-test) than that measured in s-GO-treated networks ( $110 \pm 6 \text{ s}$ , n=18  
22 cells, right plot in Figure 2 (b)). When  $\text{GABA}_A$  receptors were pharmacologically blocked by  
23 bicuculline ( $20 \mu\text{M}$ ; 20 min), an antagonist of inhibitory connections known to potentiate  
24 rhythmic activity patterns<sup>23,26,27</sup>, the control IEI average value was still significantly lower ( $P <$   
25  $0.001$ ; Student's t-test) than that measured in s-GO neurons in the presence of the  $\text{GABA}_A$   
26 receptor antagonist ( $18 \pm 1 \text{ s}$ , n = 20 control cells, vs  $92 \pm 10 \text{ s}$ , n = 18 s-GO cells; plot in Figure  
27 2 (b), right). This indicated a direct reduction in the excitatory activity due to s-GO exposure.

28 Next we recorded single cell synaptic activity in the presence of TTX ( $1 \mu\text{M}$ , Figure 3  
29 (a)). Under these experimental conditions synaptic currents, termed miniature PSCs (mPSCs),  
30 do not depend on action potential generation. mPSCs are due to the stochastic fusion of  
31 neurotransmitter vesicles at the presynaptic membrane and their frequency is proportional to the  
32 number of synaptic contacts<sup>28</sup>. Despite the fact that in the recorded hippocampal neurons  
33 spontaneous synaptic activity was manifested as inward currents (in our recording conditions,  
34 see Supporting Information<sup>21</sup>) made up by a mixed population of inhibitory ( $\text{GABA}_A$  receptor-  
35 mediated) and excitatory (AMPA glutamate receptor-mediated) PSCs, virtually all mPSCs, as  
36 previously reported<sup>21</sup>, were identified as excitatory by their fast kinetics (decay time constant  $\tau =$

1  $4 \pm 0.3$  ms, see Supporting Information<sup>22</sup>). Notably, s-GO significantly decreased ( $P < 0.001$ ,  
2 Student's t-test; see plots in Figure 3 (a)) the frequency of mPSCs without affecting their  
3 amplitude ( $0.06 \pm 0.02$  Hz and  $30 \pm 0.7$  pA, control,  $n = 15$ ;  $0.02 \pm 0.001$  Hz and  $26 \pm 0.7$  pA, s-  
4 GO-treated  $n= 9$ ; summarized in Figure 3 (a)). To ascertain whether the s-GO interference with  
5 synaptic activity was selective on glutamate-mediated fast synaptic transmission, we tested the  
6 occurrence of evoked inhibitory PSCs by pair recordings of mono-synaptically coupled neurons<sup>22</sup>  
7 (Supplementary Information and Figure S6a) and we observed that s-GO apparently did not  
8 impair GABA<sub>A</sub> mediated connections.

9         To determine whether changes in excitatory synaptic density may account for the  
10 reduction in fast- mPSC frequency detected in s-GO treated cultures, neurons were co-  
11 immunostained for  $\beta$ -tubulin III and the vesicular glutamate transporter (VGLUT1), a  
12 transmembrane protein localized at the glutamatergic presynaptic terminals<sup>29</sup>. Antibody to  
13 VGLUT1 labeled presynaptic boutons under both conditions (Figure 3b). Using  $\beta$ -tubulin III  
14 labeling to identify neuronal bodies and dendrites, we quantified VGLUT1-positive puncta,  
15 detecting a significant ( $P < 0.001$ ; Student's t-test) reduction in their density in s-GO treated  
16 samples (control  $1.4 \times 10^3 \pm 0.045 \times 10^3$   $n= 6$  fields and s-GO  $0.28 \times 10^3 \pm 0.11 \times 10^3$   $n= 6$   
17 fields, plot in Figure 3 (b)). Parallel experiments were performed to quantify GABAergic  
18 synapses, by similar co-staining but for the vesicular GABA transporter (VGAT) to localize  
19 presynaptic GABAergic terminals<sup>22,30</sup>. These studies indicated that s-GO incubation did not alter  
20 the inhibitory connection density (Supporting Information and Figure S6b).

1 **Figure 3**



2  
3 **Figure 3.** *s-GO* exposure at high concentration impaired excitatory synapses. In (a) sample tracings of mPSCs  
4 recorded in control and *s-GO*-treated cultures (left panel). Right panel: plots reporting mPSC amplitude and  
5 frequency values. *s-GO*-treatment significantly decreased the frequency of mPSCs (\*\*\*) =  $P < 0.001$  Student's-t-  
6 test). In (b) confocal reconstruction of control and *s-GO* treated neurons immunolabeled for the vesicular glutamate  
7 transporter 1 (VGLUT1; green) and counterstained for cytoskeletal component  $\beta$ -tubulin III (red; nuclei are  
8 visualized by DAPI in blue; scale bar 10  $\mu$ m). The plot shows the significant decrease of VGLUT1-positive puncta  
9 in *s-GO*-treated cultures (\*\*\*) =  $P < 0.001$  Student's-t-test). In (c) top, fluorescence images following staining with  
10 FM1-43, control and *s-GO*-treated. Scale bar 50  $\mu$ m. The areas in the boxes are higher magnifications to highlight  
11 the difference in vesicular staining between the two conditions (scale bar 100  $\mu$ m). The plot (top right) reproduces  
12 the representative (control and *s-GO*) traces of FM1-43 de-staining (please note that each trace has been normalized  
13 to the maximum fluorescence detected). Bottom: the left plot summarizes the initial raw fluorescent intensities of  
14 hippocampal terminals from control and *s-GO*-treated cultures (\*\* =  $P < 0.01$  Mann-Whitney test); the right plot  
15 summarizes the decay time constant  $\tau$  of FM1-43 de-staining in the two conditions (\*\*\*) =  $P < 0.001$ , Mann-Whitney  
16 test).  
17

1            In the next set of experiments we measured the kinetics of synaptic vesicle release by  
2 real-time imaging of vesicles labeled with FM dye to monitor the rate of presynaptic vesicle  
3 recycling from hippocampal neurons treated or untreated with s-GO. After staining with the  
4 lipophilic dye FM1-43<sup>31-33</sup> clusters of presynaptic terminals were visible as bright fluorescence  
5 spots (Figure 3 (c)). The fluorescence intensity measured on FM-positive puncta following high  
6 KCl (50 mM;<sup>34</sup>) depolarization is proportional to the number of vesicles endocytosed during  
7 synaptic vesicle recycling, and thus, allows to estimate the size of the recycling vesicle pool<sup>34</sup>. In  
8 s-GO treated cells, upon high-K<sup>+</sup>-loading protocol, we detected a significant (P < 0.01; Mann-  
9 Whitney test) reduction in the raw fluorescence intensity of FM1-43-positive hippocampal  
10 terminals (control 11876 ± 1100 arbitrary units –a.u.–, n= 7 fields; s-GO-treated 7400 ± 1057  
11 a.u., n= 6 fields; 3 different culture series; Figure 3 (c)), suggesting that chronic incubation with  
12 s-GO decreased the recycling vesicle pool. When analyzing the decay time constant ( $\tau$ ) of the  
13 FM1-43 fluorescence de-staining profiles during vesicle exocytosis, we observed a significant  
14 (P < 0.001; Mann-Whitney test) difference in the kinetics displayed by control ( $\tau$ = 5.7 ± 0.5 s, n  
15 = 205 terminals) and s-GO ( $\tau$ = 18 ± 2 s, n = 85 terminals) treated cells, as summarized in Figure  
16 3 (c). In reference experiments, image series captured on FM1-43 stained cells but without the  
17 high-K<sup>+</sup> de-staining stimulus, produced a baseline reference plot (not shown). Taken together,  
18 these results support the specific ability of chronic exposure to s-GO flakes to reduce the amount  
19 of excitatory synaptic contacts and to interfere with presynaptic vesicle recycling.

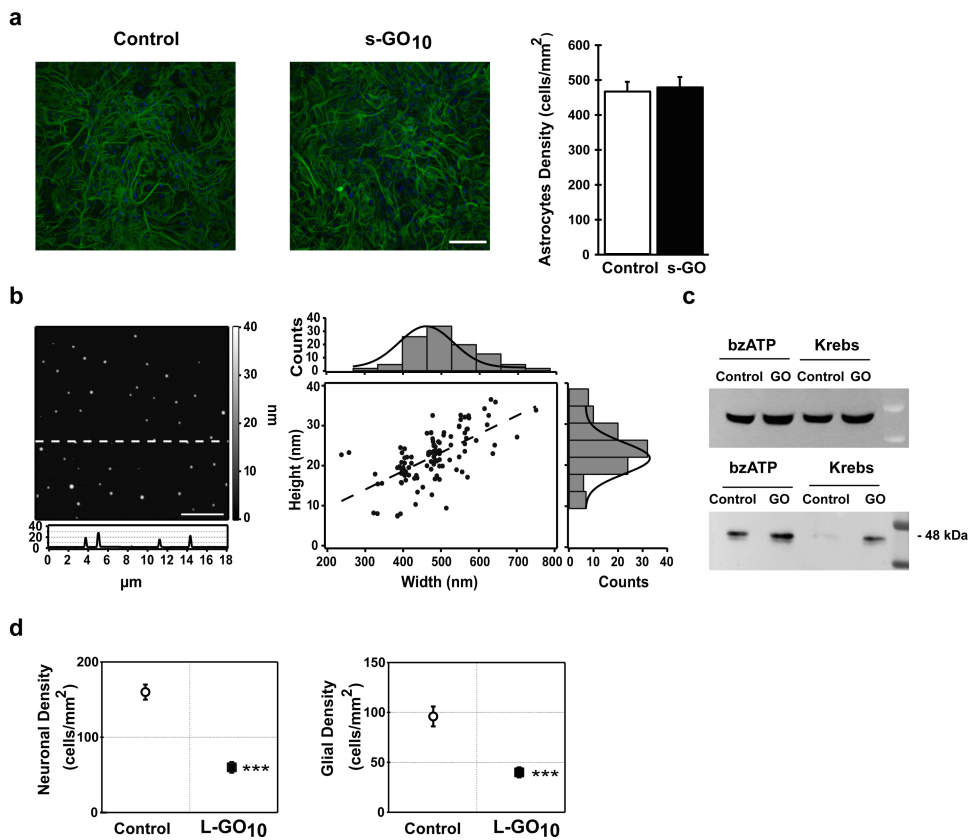
20            To test the ability of s-GO to impair cell membrane dynamics in general, we investigated  
21 whether s-GO (10  $\mu$ g/mL) was also reducing exocytosis and recycling of synaptic-like  
22 microvesicles (MVs<sup>35</sup>) from cultured primary glial cells (see Supplementary Information). MVs  
23 are released into the extracellular space by direct budding from the plasma membrane of  
24 astrocytes, and have been shown to contribute to intercellular communication<sup>15,35,36</sup>. We treated  
25 pure glial cell cultures with s-GO (10  $\mu$ g/mL) for 6-8 days. In Figure 4 (a) immunofluorescence  
26 staining of control and s-GO treated GFAP-positive cells are shown. s-GO incubation did not  
27 affect astrocyte density (Figure 4 (a) right histograms; n= 20 fields for both conditions)  
28 excluding any cytotoxic effect. In glial cultures MVs release was induced by bzATP incubation  
29 (100 $\mu$ M, 30 min, n= 3 different series of cultures<sup>37-39</sup>), and MVs release was detected and  
30 quantified by immunoblot analysis of the collected supernatant. In control, bzATP stimulation  
31 induced the appearance of the band corresponding to flotillin-1 (Figure 4 (c), bottom blot), a  
32 signature of MVs release<sup>40-42</sup>. Surprisingly, in s-GO treated astrocytes, the bzATP stimulation  
33 induced a marked increase in the size of the flotillin-1 band. This band was also detected in the  
34 absence of stimulation (Figure 4 (c) bottom blot) suggesting that s-GO *per se* induced MVs  
35 constitutive release.

1 AFM micrographs, show in Figure 4 (b) (left panel) the presence of vesicles in the  
2 stimulated control supernatant appearing as circular spots protruding from the ultra-flat mica  
3 surface. For each of them, width and height were independently measured from particle crossing  
4 height profiles and the resulting distributions were plotted (Figure 4 (b) right panel).  
5 Intriguingly, similar experiments with GR (10  $\mu\text{g}/\text{mL}$ ) did not induce shedding of MVs in glial  
6 cell cultures (Supplementary Information and Figure S7).

7 We also attempted to investigate the effect of increased lateral size of GO (l-GO, with a  
8 lateral dimension in the few  $\mu\text{m}$  range; 10  $\mu\text{g}/\text{mL}$  final concentration) on cultured hippocampal  
9 cells. However, after 6-8 days of incubation, we measured a significant ( $P < 0.001$ ; Student's t-  
10 test; Figure 4 (d)) reduction in both neuron and glial cell densities (control  $160 \pm 10$   
11 neurons/ $\text{mm}^2$  and  $96 \pm 10$  astrocytes/ $\text{mm}^2$ ; l-GO-treated  $96 \pm 10$  neurons/ $\text{mm}^2$  and  $40 \pm 7$   
12 astrocytes/ $\text{mm}^2$ ; n=10 visual fields each, 3 series of cultures; Figure 4 (d)) indicating cell toxicity  
13 that prevented any further functional measurements. We believe further investigations are  
14 warranted to explore such lateral size-dependent cytotoxic responses.

15  
16  
17  
18  
19  
20  
21  
22

1 **Figure 4**



2  
3  
4  
5  
6  
7  
8  
9  
10  
11  
12  
13  
14  
15  
16  
17  
18

**Figure 4.** *s-GO* exposure and microvesicles release in glial cells. In (a) immunolabeling of primary rat astrocytes (3 weeks) in control and *s-GO* treated cells (10  $\mu\text{g}/\text{mL}$  6-8 days). Both cultures were immune-stained for GFAP (green) and nuclei visualized by DAPI (blue; scale bar: 100  $\mu\text{m}$ ). No statistical significance was found between the two conditions (top right). In (b) AFM image of fixed MVs where the differences in color are representative of height differences (brighter means higher). A representative height profile crossing 3 MVs is reported. The scatter plot (right) shows MVs width versus height distribution and is fitted with a regression line represented by the equation  $y = 0.046x + 0.218$ . A frequency histogram, built upon experimental measurements of both width and height, was plotted over each axis of the scatter graph, and fitted with Gaussian distributions. The frequency histograms revealed the highest number of occurrences to be about 490 nm and 24 nm for width and height, respectively. In (c) Western blotting of the pellets (bottom row) and cell lysates (top row) for the MVs marker flotillin-1. Pellets were obtained from the medium of glial cultures treated or un-treated with *s-GO*, under 2 different conditions: stimulated and not stimulated (Krebs) by 100  $\mu\text{M}$  BzATP. Note the marked increase of the band for flotillin-1 in *s-GO* treated cells. In (d) plots summarizing the decreased density of hippocampal cells when treated with L-GO ( $\sim 10 \mu\text{m}$  lateral size; 10  $\mu\text{g}/\text{mL}$  final concentration).

1           We report here the ability of s-GO nanosheets to interfere specifically with neuronal  
2 synapses, without affecting cell viability. In particular, in cultured neuronal networks, upon  
3 chronic s-GO exposure, glutamatergic release sites were sized down. This was shown by: i) the  
4 reduction in frequency of spontaneous synaptic activity (PSCs and mPSCs) together with the  
5 marked reduction in VGLUT1-positive labeling<sup>43</sup>, ii) the reduced probability of finding active  
6 neurons when network were explored by Ca<sup>++</sup>-imaging<sup>23,44</sup> and iii) the decreased recycle vesicle  
7 pool quantified by FM1-43 measures together with the altered kinetic of vesicle recycling<sup>34</sup>.  
8 This down-regulation of glutamate-mediated synapses was apparently not due to a general cell-  
9 membrane disruption or to neuronal cell loss. In fact, we never detected alterations in basic  
10 electrophysiological parameters, reflecting neuronal health and membrane integrity<sup>18-20</sup>.

11           In addition, cell densities in treated cultures were comparable to control ones. The  
12 survival of GFAP-positive glial cells was also not affected by s-GO exposure, both in mixed  
13 neuronal and in pure neuroglial cultures. In the latter condition, MVs release was indirectly  
14 monitored by the blot analysis of flotillin-1 protein<sup>40,41</sup>, and MVs presence confirmed by direct  
15 AFM measures. In these cultures, exposure to s-GO stimulated the basal release of shed vesicles  
16 and augmented the bzATP-induced one<sup>37-39</sup>. s-GO increase in MVs release from neuroglia cells  
17 might be related to a general cell-stress condition<sup>15</sup> ultimately due to s-GO glial-membrane  
18 interactions or even internalization, depending on the flakes' shape, lateral dimension and  
19 oxidization degree<sup>10</sup> as well as the degree of protein adsorption from the culturing milieu<sup>45</sup>.

20           Based on our experimental evidence we cannot rule out that treatment with s-GO down  
21 regulated the synaptic function (in particular presynaptic release) via MVs released in mixed  
22 neuronal-glia cultures, thus excluding a direct, membrane interference of s-GO nanosheets at  
23 the pre-synaptic glutamatergic terminals. MVs have long been reported as active messengers of  
24 intercellular communication, rather than mere inert debris<sup>37</sup>, however, to our knowledge, there  
25 are no reports of astrocyte shed-MVs acting as regulators of synaptic activity. On the contrary,  
26 MVs released by microglia have been reported to affect synaptic activity, mainly acting at the  
27 presynaptic site of the excitatory synapses, but increasing synaptic activity and release in  
28 primary cultures<sup>37</sup>. Against this neuroglial-cell mediated response to s-GO is also the fact that  
29 astrocyte density in mixed cultures is artificially kept at a low level by the culturing procedure in  
30 itself, while the surviving microglia are even fewer<sup>46</sup>.

1           In contrast to s-GO, the inert nature of GR flakes regarding synaptic activity and MVs  
2 release by glia is also of interest. This could be due to differences in shape and lateral size  
3 affecting flake-membrane interactions<sup>10</sup>. It is also interesting to consider that GR have a much  
4 less hydrophilic surface character and overall poorer dispersibility in cell culture media<sup>45</sup> that  
5 may lead to the formation of aggregates potentially unable to interact with sub-microscopic  
6 structures (such as the synaptic clefts).

7           The apparent selectivity in terms of the presynaptic terminals targeted by s-GO was also  
8 notable, with the inhibitory, GABAergic ones that remained unaffected, as evidenced by pair  
9 recordings and the VGAT labeling<sup>22</sup>. Given the ability of graphene flakes to undergo motion and  
10 vibration that can lead to interaction with and possible piercing of lipid bilayers<sup>8</sup>, we propose an  
11 alternative mechanistic interpretation of our synaptic results. s-GO flakes may prevent the  
12 synaptic vesicle endocytotic cycle because their dimensions allow them to interact with the  
13 presynaptic cell membrane at the periphery of the synaptic cleft and then be up-taken by  
14 vesicles. In this process, the flakes may transiently trap vesicles in an open mode and prevent  
15 their closing and the subsequent endocytosis. This could affect synaptic release in the short term  
16 inducing, in the long term, a down regulation of glutamatergic release sites and synapses. To  
17 note, glutamatergic synaptic activity is specifically affected also when neurons are transiently  
18 exposed to s-GO, with a short-term up-regulation of release, turned into a down regulation  
19 within the first 3 days of chronic exposure (Figure S8 in Supplementary Information). The  
20 mechanism of such interaction among s-GO flakes and vesicles could be similar to what has  
21 been previously described for dispersed single walled carbon nanotubes<sup>47</sup>. In this context, the  
22 unlikelihood of affecting GABAergic terminals may reside in the different dimensions of the  
23 excitatory (16 nm) and inhibitory (10 nm) synaptic clefts<sup>48</sup>. The latter reported to be even  
24 narrowed to 6 nm at the periphery of the clefts due to transcleft elements while docked vesicles  
25 are concentrated at the central cleft domain<sup>48</sup>. On the contrary, docked vesicles in excitatory  
26 synapses are distributed evenly over the synaptic cleft<sup>48</sup>. It is tempting to speculate that these  
27 synaptic ultra-structural differences might explain why glutamatergic terminals became ideal  
28 targets to s-GO interactions. This selectivity is supported by the notion that, even when  
29 transiently exposed to s-GO via pressure ejected brief pulses, GABAergic synapses are  
30 unaffected (see Supplementary Information).



1           Regardless of the mechanisms involved, the ability of s-GO to alter synapses and induce  
2 glial cell reaction has not been previously documented. This might compromise neuronal  
3 signaling and CNS functions and seems crucially dependent on the GO sheet dimensions, since  
4 larger flakes were found unequivocally cytotoxic. In our experiments 6 days exposure of cultures  
5 to equal amounts of dispersed l-GO induced unequivocal hippocampal cell loss, both neuroglia  
6 and neurons, thus hampering any further evaluation of membrane/flakes interactions.  
7 These observations deserve further studies, in fact, altering synapses and inducing glia reactivity  
8 may raise concerns from the safety and nanotoxicity point of view<sup>49</sup>.

9           Beyond the safe design of nanomaterials, such a subtle interference affecting exquisite  
10 CNS signaling may offer possibilities in neuropharmacology, when specific targeting of  
11 excitatory synapses is desired<sup>50-52</sup>. The use of nanoparticles as therapeutics is in fact fueled by  
12 their ability to circumvent biological barriers<sup>53</sup> and targeting of synapses has created the basis for  
13 theranostics applications<sup>54</sup>. Our observations with thin s-GO flakes illustrate the potential of 2D  
14 nanosheet physical properties to engineer novel and specific glutamate-transmission modulators.  
15 It is also relevant to note that synapse formation and function in neuronal networks, when  
16 interfaced to planar graphene-based materials, are not affected<sup>55</sup>. This strengthens the notion that  
17 when exploring the application of graphene in biology, studies should be performed with well-  
18 characterized types of materials, since the materials' physical-chemical features, including  
19 geometry, are governing the potential interactions with specific biological components<sup>2</sup>.

## 20 21 **Methods**

22 Materials and Methods are described in the Associated Content and Figures

## 23 24 **ASSOCIATED CONTENT**

25 **Supporting Information:** Materials and Methods, Supporting Results, Figure S1- S8 and  
26 Tables S1-S2.

## 27 28 **AUTHOR INFORMATION**

### 29 **Corresponding Author**

30 \* Laura Ballerini International School for Advanced Studies (SISSA) via Bonomea 265 I-34136  
31 Trieste phone +39 0403787779, LB [laura.ballerini@sissa.it](mailto:laura.ballerini@sissa.it)

## 1 **Author Contributions**

2 R.R. and A.F. performed cell biology, electrophysiology and immunofluorescence experiments  
3 and analysis; R.R. and F.P.U.S. design and performed imaging and real-time imaging  
4 experiments and analysis; N.L. and K.K. contributed to the synthesis and characterization of  
5 thin graphene oxide (l-GO and s-GO) of biological-grade; V.L. and E.V. contributed to the  
6 synthesis and characterization of pristine graphene (GR); M.M. performed glial cell  
7 experiments, immunofluorescence and western blot; D.S., I.R. and L.C. designed and  
8 performed the AFM experiments; L.B. and M.P. conceived the study; L.B. conceived the  
9 experimental design and contributed to the analysis of data; L.B. wrote the manuscript. All  
10 authors have given approval to the final version of the manuscript.

## 11 **Funding Sources**

12 We acknowledge financial support from the EU FP7-ICT-2013-FET-F GRAPHENE Flagship  
13 project (no. 604391), from the NEUROSCAFFOLDS-FP7-NMP-604263 and PRIN-MIUR n.  
14 2012MYESZW.  
15

## 16 **Notes**

17 The authors declare no competing financial interest.  
18  
19

## 20 **ACKNOWLEDGMENTS**

21 We are especially grateful to Micaela Grandolfo, Jessica Franzot and Beatrice Pastore for supervising  
22 the synaptic immune staining and quantification, the glial cell culturing and western blot experiments.  
23 IOM-TASC national laboratory (Trieste) is also gratefully acknowledged for AFM assistance. N.L.  
24 acknowledges Leon Newman for assistance with the TEM and Raman instrumentation. X-ray  
25 photoelectron spectra were performed at the National EPSRC XPS User's Service (NEXUS) at  
26 Newcastle University, an EPSRC Mid-Range Facility. N.L. acknowledges Mr. Leon Newman for  
27 assistance with the TEM and Raman instrumentation and Dr Nigel Hodson of the University of  
28 Manchester BioAFM Facility for his expert advice. The Antolin Group is also acknowledged for the  
29 provision of the commercial material. We acknowledge financial support from the EU FP7-ICT-2013-  
30 FET-F GRAPHENE Flagship project (no. 604391), from the NEUROSCAFFOLDS-FP7-NMP-604263  
31 and PRIN-MIUR n. 2012MYESZW.  
32

## 33 **REFERENCES**

- 34 1. Sanchez, V.C.; Jachak, A.; Hurt, R.H.; Kane, A.B. *Chem Res Toxicol.* **2012**, *25*, 15-34.
- 35 2. Kostarelos, K.; Novoselov, K.S. *Science* **2014**, *344*, 261-263.
- 36 3. Mao, H.Y.; Laurent, S.; Chen, W.; Akhavan, O.; Imani, M.; Ashkarran, A.A.; Mahmoudi,  
37 M. *Chem Rev.* **2013**, *113*, 3407-3424.

- 1 4. Bitounis, D.; Ali-Boucetta, H.; Hong, B.H.; Min, D.H.; Kostarelos, K. *Adv Mater.* **2013**,
- 2 25, 2258-2268.
- 3 5. Krishna, K.V.; Ménard-Moyon, C.; Verma, S.; Bianco, A. *Nanomedicine (Lond)* **2013**, 8,
- 4 1669-1688.
- 5 6. Wang, Y.; Li, Z.; Wang, J.; Li, J.; Lin, Y. *Trends Biotechnol.* **2011**, 29, 205-212.
- 6 7. Kuzum, D.; Takano, H.; Shim, E.; Reed, J.C.; Juul, H.; Richardson, A.G.; de Vries, J.; Bink,
- 7 H.; Dichter, M.A.; Lucas, T.H.; Coulter, D.A.; Litt Li, B. *Nat Commun.* **2015**, 5, 5259-
- 8 5263.
- 9 8. Li, Y.; Yuan, H.; von dem Bussche, A.; Creighton, M.; Hurt, R.H.; Kane, A.B.; Gao, H.
- 10 *Proc Natl Acad Sci U S A.* **2013**, 110, 12295-12300.
- 11 9. Tu, Y.; Lv, M.; Xiu, P.; Huynh, T.; Zhang, M.; Castelli, M.; Liu, Z.; Huang, Q.; Fan, C.;
- 12 Fang, H.; Zhou, R. *Nat Nanotechnol.* **2013**, 8, 594-601.
- 13 10. Mao, J.; Guo, R.; Yan, L. *Biomaterials* **2014**, 35, 6069-6077.
- 14 11. Rizzoli, S.O. *EMBO J.* **2014**, 33, 788-822.
- 15 12. Bianco, A. *Angew Chem Int Ed Engl.* **2013**, 52, 4986-4997.
- 16 13. Yang, D.; Li, T.; Xu, M.; Gao, F.; Yang, J.; Yang, Z.; Le, W. *Nanomedicine (Lond)* **2014**,
- 17 9, 2445-2455.
- 18 14. Zhang, Y.; Ali, S.F.; Dervishi, E.; Xu, Y.; Li, Z.; Casciano, D.; Biris, A.S. *ACS Nano*
- 19 **2010**, 4, 3181-3186.
- 20 15. Falchi, A.M.; Sogos, V.; Saba, F.; Piras, M.; Congiu, T.; Piludu, M. *Histochem Cell Biol.*
- 21 **2013**, 139, 221-231.
- 22 16. León, V.; Quintana, M.; Herrero, M.A.; Fierro, J.L.; de la Hoz, A.; Prato, M.; Vázquez, E.
- 23 *ChemCommun (Camb).* **2011**, 47, 10936-10938
- 24 17. León, V.; Rodriguez, A.M.; Prieto, P.; Prato, M.; Vázquez, E. *ACS Nano* **2014**, 8, 563-571
- 25 18. Carp, J.S. *J Neurophysiol.* **1992**, 68, 1121-1132.
- 26 19. Gao, Y.; Liu, L.; Li, Q.; Wang, Y. *NeurosciLett.* **2015**, 591, 138-143.
- 27 20. Djuric, U.; Cheung, A.Y.; Zhang, W.; Mok, R.S.; Lai, W.; Piekna, A.; Hendry, J.A.; Ross,
- 28 P.J.; Pasceri, P.; Kim, D.S.; Salter, M.W.; Ellis, J. *Neurobiol Dis.* **2015**, 76, 37-45.
- 29 21. Lovat, V.; Pantarotto, D.; Lagostena, L.; Cacciari, B.; Grandolfo, M.; Righi, M.; Spalluto,
- 30 G.; Prato, M.; Ballerini, L. *Nano Lett.* **2005**, 5, 1107-1110.
- 31 22. Cellot, G.; Toma, F.M.; Varley, Z.K.; Laishram, J.; Villari, A.; Quintana, M.; Cipollone, S.;
- 32 Prato, M.; Ballerini, L. *J Neurosci.* **2011**, 31, 12945-12953.
- 33 23. Bosi, S.; Rauti, R.; Laishram, J.; Turco, A.; Lonardoni, D.; Nieuws, T.; Prato, M.; Scaini, D.;
- 34 Ballerini, L. *Sci Rep.* **2015**, 5, 9562.
- 35 24. Stetter, O.; Battaglia, D.; Soriano, J.; Geisel, T. *PLoSComput Biol.* **2012**, 8.
- 36 25. Fabbro, A.; Pastore, B.; Nistri, A.; Ballerini, L. *Cell Calcium.* **2007**, 41, 317-329.

- 1 26. Tibau, E.; Valencia, M.; Soriano, J. *Front Neural Circuits* **2013**, 7, 199.
- 2 27. Sokal, D.M.; Mason, R.; Parker, T.L. *Neuropharmacology* **2000**, 39, 2408-2417.
- 3 28. Raastad, M.; Storm, J.F.; Andersen, P. *Eur J Neurosci*.**1992**, 4, 113-117
- 4 29. Bellocchio, E.E.; Reimer, R.J.; Freneau, R.T., Jr; Edwards, R.H. *Science* **2000**, 289, 870-
- 5 876.
- 6 30. Moulder, K.L.; Jiang, X.; Taylor, A.A.; Shin, W.; Gillis, K.D.; Mennerick S. *J Neurosci*.
- 7 **2007**, 27, 9846-9854.
- 8 31. Betz, W.J.; Bewick, G.S. *Science* **1982**, 255, 200-203
- 9 32. Ryan, T.A.; Reuter, H.; Wendland, B.; Schweizer, F.E.; Tsien, R.W.; Smith, S.J. *Neuron*.
- 10 **1993**, 11, 713-724.
- 11 33. Betz, W.; Mao, F.; Smith, C. *Curr Opin Neurobiol*. **1996**, 6, 365-371.
- 12 34. Ryan, T.A. *Curr Opin Neurobiol*. **2001**, 11, 544-549.
- 13 35. Turola, E.; Furlan, R.; Bianco, F.; Matteoli, M.; Verderio, C. *Front Physiol*. **2012**, 3:149.
- 14 36. Frühbeis, C.; Fröhlich, D.; Kuo, W.P.; Krämer-Albers, E.M. *Front Cell Neurosci*. **2013**, 7,
- 15 182.
- 16 37. Antonucci, F.; Turola, E.; Riganti, L.; Caleo, M.; Gabrielli, M.; Perrotta, C.; Novellino, L.;
- 17 Clementi, E.; Giussani, P.; Viani, P.; Matteoli, M.; Verderio, C. *EMBO J*. **2012**, 31, 1231-
- 18 1240.
- 19 38. Bianco, F.; Pravettoni, E.; Colombo, A.; Schenk, U.; Möller, T.; Matteoli, M.; Verderio, C.
- 20 *J Immunol*. **2005**, 174, 7268-7277.
- 21 39. Bianco, F.; Perrotta, C.; Novellino, L.; Francolini, M.; Riganti, L.; Menna, E.; Saglietti, L.;
- 22 Schuchman, E.H.; Furlan, R.; Clementi, E.; Matteoli, M.; Verderio C. *EMBO J*. **2009**, 28,
- 23 1043-1054
- 24 40. Del Conde, I.; Shrimpton, C.N.; Thiagarajan, P.; López, J.A. *Blood* **2005**, 106, 1604-1611.
- 25 41. Al-Nedawi, K.; Meehan, B.; Micallef, J.; Lhotak, V.; May, L.; Guha, A.; Rak, J.; *Nat Cell*
- 26 *Biol*. **2008**, 10, 619-624.
- 27 42. Antonyak, M.A.; Cerione, R.A. *Methods Mol Biol*. **2014**, 1165,147-173.
- 28 43. Toyoshima, D.; Mandai, K.; Maruo, T.; Supriyanto, I.; Togashi, H.; Inoue, T.; Mori, M.;
- 29 Takai, Y. *PLoS One*. **2014**, 27, 9-e89763.
- 30 44. Aguado, F.; Carmona, M.A.; Pozas, E.; Aguiló, A.; Martínez-Guijarro, F.J.; Alcantara, S.;
- 31 Borrell, V.; Yuste, R.; Ibañez, C.F.; Soriano, E. *Development* **2003**, 130, 1267-1280.
- 32 45. Chong, Y.; Ge, C.; Yang, Z.; Garate, J.A.; Gu, Z.; Weber, J.K.; Liu, J.; Zhou, R. *ACS Nano*.
- 33 **2015**, 9, 5713-5724.

- 1 46. Fabbro, A.; Sucapane, A.; Toma, F.M.; Calura, E.; Rizzetto, L.; Carrieri, C.; Roncaglia, P.;  
2 Martinelli, V.; Scaini, D.; Masten, L.; Turco, A.; Gustincich, S.; Prato, M.; Ballerini, L.  
3 *PLoS One*. **2013**, 8(8):e73621.
- 4 47. Malarkey, E.B.; Reyes, R.C.; Zhao, B.; Haddon, R.C.; Parpura, V. *Nano Lett.* **2008**, 8,  
5 3538-3542.
- 6 48. High, B.; Cole, A.A.; Chen, X.; Reese, T.S. *Front Synaptic Neurosci.* **2015**, 7, 9.
- 7 49. Fedorovich, S.V.; Alekseenko, A.V.; Waseem, T.V. *Biochem Soc Trans.* **2010**, 38, 536-  
8 538.
- 9 50. Grados, M.A.; Atkins, E.B.; Kovacicova, G.I.; McVicar, E. *Psychology Res and Behavior*  
10 *Management PRBM* **2015**, 8, 115-131.
- 11 51. Gardoni, F.; Di Luca, M. *Curr Opin in Pharmacology* **2015** 20, 24-28.
- 12 52. Stone, J.M., *Ther Adv Psychopharmacol.* **2011**, 1, 5-18.
- 13 53. Meyer, R.A.; Sunshine, J.C.; Green, J.J. *Trends Biotechnol.* **2015**, 33, 514-524.
- 14 54. Borisova, T.; Nazarova, A.; Dekaliuk, M.; Krisanova, N.; Pozdnyakova, N.; Borysov, A.;  
15 Sivko, R.; Demchenko, A.P. *Int J Biochem Cell Biol.* **2015**, 59, 203-215.
- 16 55. Fabbro A.; Scaini D.; León V.; Vázquez E.; Cellot G.; Privitera G.; Lombardi L.;  
17 Torrisi F.; Tomarchio F.; Bonaccorso F.; Bosi S.; Ferrari A.C.; Ballerini L.; Prato M. *ACS*  
18 *Nano.* **2016**, 10, 615-23.
- 19